Inorganic Chemistry

pubs.acs.org/IC Article

Iron(III)−Oxo Cluster Chemistry with Dimethylarsinate Ligands: Structures, Magnetic Properties, and Computational Studies

Kenneth Hong Kit Lee, Juan E. Peralta, Khalil A. Abboud, and George Christou*

Cite This: *Inorg. Chem.* 2020, 59, 18090−18101 Read Online

ACCESS | Metrics & More | Article Recommendations | Supporting Information

ABSTRACT: A program has been initiated to develop Fe^{III}/oxo cluster chemistry with the "pseudocarboxylate" ligand dimethylarsinate ($Me_2AsO_2^-$) for comparison with the well investigated Fe^{III}/oxo/carboxylate cluster area. The synthesis and characterization of three polynuclear Fe^{III} complexes are reported, $[Fe_{12}O_4(O_2C^tBu)_8(O_2AsMe_2)_{17}(H_2O)_3]Cl_3$ (**1**), $Na_2[Fe_{12}Na_2O_4(O_2AsMe_2)_{20}(NO_3)_6(Me_2AsO_2H)_2(H_2O)_4](NO_3)_6$ (**2**), and $[Fe_3(O_2AsMe_2)_6(Me_2AsO_2H)_2(hqn)_2](NO_3)$ (**3**), where hqnH is 8-hydroxyquinoline. The Fe_{12} core of **1** is a type never previously encountered in Fe^{III} carboxylate chemistry, consisting of two Fe_6 units each of which comprises two $\{Fe_3(\mu_3\text{-}O^{2-})\}$ units bridged by three $Me_2AsO_2^-$ groups and linked into an Fe_{12} loop structure by two *anti*−*anti* $\eta^1{:}\eta^1{:}\mu$ $Me_2AsO_2^-$ groups, a bridging mode extremely rare with carboxylates. **2** also consists of two Fe_6 units, differing in their ligation from those in **1**, and this time linked together into a linear structure by a central $\{Na_2(NO_3)_2\}$ bridging unit. **3** is a linear Fe_3 complex with no monatomic bridges between Fe^{III} ions, a very rare situation in Fe^{III} chemistry with any ligands and unprecedented in Fe carboxylate chemistry. The distinct differences observed in arsinate vs carboxylate ligation modes are rationalized largely based on the greater basicity of the former vs the latter. Variable-temperature dc and ac magnetic susceptibility data reveal all Fe_2 pairwise interactions to be antiferromagnetic. For **1** and **2**, the different J_{ij} couplings were estimated by use of a magnetostructural correlation for high nuclearity Fe^{III}−oxo clusters and by density functional theory calculations using broken symmetry methods, allowing identification of their relative spin vector alignments and thus rationalization of their $S = 0$ ground states. The J_{ij} values were then used as input values to give excellent fits of the experimental $\chi_M T$ vs T data. For **3**, the fits of the experimental $\chi_M T$ vs T data to the Van Vleck equation or with PHI gave a very weak $J_{12} = -0.8(1)$ cm^{-1} ($H = -2J\hat{S}_i\cdot\hat{S}_j$ convention) between adjacent Fe^{III} ions and an $S = {}^5/_2$ ground state. These initial Fe^{III} arsinate complexes also provide structural parameters that help validate literature assignments of arsinate binding modes to iron oxide/hydroxide minerals as part of environmental concerns of using arsenic-containing herbicides in agriculture.

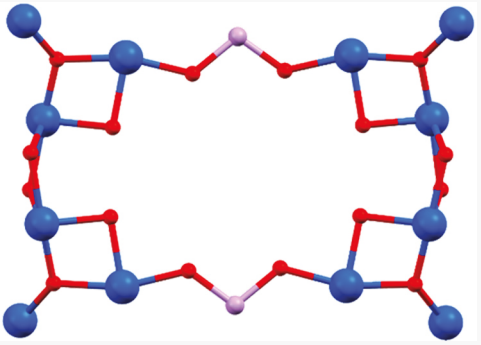

INTRODUCTION

Iron^{III}−oxo cluster chemistry has been the subject of investigation by many research groups around the world for many years because of the relevance of this field to a wide range of areas. These include molecular magnetism and single-molecule magnets and associated effects such as spin frustration,[1−3] bioinorganic chemistry involving structural models of various Fe proteins and enzymes,[4,5] materials chemistry, such as iron-based Keggin ions that are the building blocks of ferrihydrite minerals,[6−8] and others. The high Lewis acidity of Fe^{III} favors formation of oxide-bridged Fe_x cores through hydrolysis, and commonly employed organic ligands on the molecule's periphery are carboxylates, either alone or in conjunction with one or more chelating/bridging groups taking advantage of the versatility of carboxylate ligands and their variety of binding and bridging modes. Using such a strategy, a multitude of Fe−oxo clusters has been prepared over the years, including such examples from our own group as $[Fe_{18}(pd)_{12}(pdH)_{12}(O_2CPh)_6(NO_3)_6](NO_3)_6$ (pdH_2 = propane-1,3-diol), which is the largest single-stranded homometallic iron wheel and $[Fe_{22}O_{14}(OH)_3(O_2CMe)_{21}(mda)_6](ClO_4)_2$ (mdaH = *N*-(methyl)diethanolamine), which is one of the largest Fe^{III}−oxo clusters reported to date.[9,10]

In recent years we have also become interested in other groups that can ligate similarly to carboxylates and which can thus be referred to as pseudocarboxylates. These have the formula $[R_xYO_y]^{-z}$ where Y = P, S, Se, or As, $x = 1$ or 2, $y = 2$ or 3, and $z = 1$ or 2. Examples include diphenylphosphinate ($Ph_2PO_2^-$), benzeneseleninate ($PhSeO_2^-$), and dimethylarsinate ($Me_2AsO_2^-$). Our own group concentrated to date in the use of these types of pseudocarboxylates in Mn−oxo cluster chemistry to investigate the result of carboxylate substitution

Received: August 26, 2020
Published: December 8, 2020

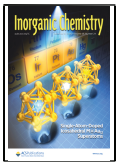

https://dx.doi.org/10.1021/acs.inorgchem.0c02554
Inorg. Chem. 2020, 59, 18090−18101

Table 1. Crystal Data and Structure Refinement Parameters for 1−3

parameter	1·15MeCN	2·2MeCN·2H$_2$O	3·4MeOH
formula[a]	$C_{74}H_{180}As_{17}Cl_3Fe_{12}O_{57}$	$C_{44}H_{142}As_{22}Fe_{12}N_{12}Na_4O_{88}$	$C_{34}H_{62}As_8Fe_3N_3O_{21}$
Fw, g mol^{-1}	4032.37	4658.00	1615.78
space group	$P2_1/c$	$P2_1/c$	$C2/c$
a (Å)	13.6281(5)	11.5569(4)	11.4773(6)
b (Å)	33.6535(12)	24.0559(9)	27.6361(13)
c (Å)	38.3252(14)	28.2647(10)	20.1457(10)
α (deg)	90	90	90
β (deg)	97.8612(8)	98.5260(10)	103.267(2)
γ (deg)	90	90	90
V, Å^3	17412.0(11)	7771.1(5)	6219.4(5)
λ, Å[b]	0.71073	0.71073	0.71073
T (K)	100(2)	100(2)	100(2)
ρ_{calc}, g/cm^3	1.543	2.067	1.694
R_1[c,d]	0.0740	0.0424	0.0377
wR_2[e]	0.1714	0.0879	0.0763

[a]Excluding solvent molecules. [b]Graphite monochromator. [c]$I > 2\sigma(I)$. [d]$R_1 = 100\sum(||F_o| - |F_c||)/\sum|F_o|$. [e]$wR_2 = 100[\sum[w(F_o^2 - F_c^2)^2]/\sum[w(F_o^2)^2]]^{1/2}$, $w = 1/[\sum^2(F_o^2) + [(ap)^2 + bp]$, where $p = [\max(F_o^2, 0) + 2F_c^2]/3$.

reactions of their conjugate acids on the well-known SMM $[Mn_{12}O_{12}(O_2CMe)_{12}(H_2O)_4]$; and it became clear that pseudocarboxylates can sometimes give similar clusters to carboxylates, but they can also be a fruitful source of new cluster types.[11−17]

Based on all the above considerations, we have initiated an investigation of Fe cluster chemistry with pseudocarboxylate ligands. This field is not well explored, and most previous work has been concentrated in alkyl(aryl)phosphonic acids (RPO_3H_2, i.e., not phosphinic acids) giving, e.g., $[Fe_{12}O_8(O_2CPh)_{14}(C_{10}H_{17}PO_3H)_6]$, $[Fe_6O_4(O_2CCMe_3)_8(O_3PPh)_2(H_2O)_2]$, and $[Fe_4OCl(O_2CMe)_3(O_3PC_6H_9)_3(py)_5]$.[18−20] For other pseudocarboxylates such as $R_2AsO_2^-$, there is a great deal of room for exploration since only some dinuclear Fe^{III}−oxo clusters have been reported.[21−23] Here we describe the initial use of dimethylarsinic acid (Me_2AsO_2H) in Fe cluster chemistry. With a high pK_a of 6.27 its conjugate base $Me_2AsO_2^-$ is a much stronger base than common carboxylates.[24−27] In Mn−oxo chemistry, Chakov et al. reported that Me_2AsO_2H can disrupt the Mn_{12} core to give the $[Mn_4O_4(O_2AsMe_2)_6]$ cubane or heterometallic $[Mn_{16}M_4O_8(O_2CPh)_{16}(O_2AsMe_2)_{24}]$ (M = Ca, Sr) with an unusual looplike structure,[17] so its products with Fe were of interest for comparison.

We were also intrigued by the fact that dimethylarsinic acid (also known as cacodylic acid) has long been used as an herbicide in growing cotton and fruit and nut trees[28,29] and the subsequent environmental concerns of its toxicity and accumulation in the soil. Several studies have found that it tends to be absorbed on iron oxide minerals in the soil;[30,31] iron oxide minerals such as goethite and ferrihydrite, as well as iron oxide nanoparticles, are known as good absorbents for As(V) compounds.[32−34] However, attempts to identify the binding modes of cacodylic acid and/or cacodylate on Fe oxides by X-ray absorption spectroscopy are hampered by the poorly explored state of Fe/O/$Me_2AsO_2^-$ chemistry, a situation that can be remedied by the availability of well characterized Fe/O/$Me_2AsO_2^-$ clusters, but these have not been available. We herein report the syntheses, crystal structures, and magnetic properties of Fe_3 and Fe_{12} clusters with $Me_2AsO_2^-$ ligation, opening up a new area of higher nuclearity Fe/O/arsinate chemistry.

EXPERIMENTAL SECTION

Syntheses. All manipulations were performed under aerobic conditions using chemicals and solvents as received, unless otherwise stated. $[Fe_3O(O_2C^tBu)_6(H_2O)_3]Cl$ and $[Fe_3O(O_2CMe)_6(H_2O)_3]Cl$ were prepared as described elsewhere.[35,36] Other reagents were commercially available; hqnH is 8-hydroxyquinoline.

$[Fe_{12}O_4(O_2C^tBu)_8(O_2AsMe_2)_{17}(H_2O)_3]Cl_3$ (1). To a stirred orange suspension of $[Fe_3O(O_2C^tBu)_6(H_2O)_3]Cl$ (0.24 g, 0.25 mmol) in MeCN (20 mL) was added Me_2AsO_2H (0.14 g, 1.0 mmol), and the mixture stirred overnight at ambient temperature. The resultant clear dark orange solution was filtered, and the filtrate was left undisturbed to slowly concentrate by evaporation by ∼20% of its volume. X-ray quality orange platelike crystals of **1**·15MeCN slowly grew over 5 days, and these were collected by filtration, washed with MeCN and Et_2O, and dried under vacuum. The yield was 31% based on As. Anal. Calcd (found) for **1** (solvent-free; $C_{74}H_{180}As_{17}Cl_3Fe_{12}O_{57}$): C, 22.04 (22.60); H, 4.50 (5.01); N, 0.00 (0.00). Selected IR data (KBr disk, cm^{-1}): 425(m), 469(s), 581(w), 603(w), 811(vs), 1225(w), 1420(s), 1483(s), 1544(s), 2960(m), 3377(br). The same reaction with $[Fe_3O(O_2CMe)_6(H_2O)_3]Cl$ gave the analogous product to **1**, as judged by IR spectral comparison.

$Na_2[Fe_{12}Na_2O_4(O_2AsMe_2)_{20}(NO_3)_6(Me_2AsO_2H)_2(H_2O)_4](NO_3)_6$ (2). To a stirred orange suspension of $Fe(NO_3)_3·9H_2O$ (0.61 g, 1.5 mmol) in MeCN (20 mL) was added solid $NaO_2AsMe_2·3H_2O$ (0.41 g, 3.0 mmol), and the reaction mixture was stirred for 3 h during which time some orange precipitate formed. The mixture was filtered, and the filtrate was left undisturbed to slowly concentrate by evaporation by ∼20% of its volume. X-ray quality orange rodlike crystals of **2**·2MeCN·2H$_2$O grew over 2 days, and these were collected by filtration, washed with MeCN and Et_2O, and dried under vacuum. The yield was 25% based on Fe. Anal. Calcd (found) for **2**: (solvent-free; $C_{44}H_{142}As_{22}Fe_{12}Na_4N_{12}O_{88}$): C, 11.35 (11.50); H, 3.07 (3.54); N, 3.61 (3.14). Selected IR data (KBr disk, cm^{-1}): 465(m), 534(w), 649(w), 832(vs), 1050(w), 1384(vs), 1638(m), 3406(br).

$[Fe_3(O_2AsMe_2)_6(hqn)_2(Me_2AsO_2H)_2](NO_3)$ (3). Me_2AsO_2H (0.34 g, 2.5 mmol) and hqnH (0.10 g, 0.70 mmol) were dissolved with stirring in MeOH (20 mL), and then NEt_3 (0.42 mL, 3.0 mmol) was added followed by the addition of $Fe(NO_3)_3·9H_2O$ (0.40 g, 1.0 mmol) to give an essentially black solution. The reaction mixture was stirred for a further 3 h and filtered, and the filtrate was layered with an Et_2O/hexanes (1:1 v/v) mixture. Black platelike crystals of **3**·4MeOH slowly grew over 5 days, and these were collected by filtration, washed with MeOH and Et_2O, and dried under vacuum. The yield was 26% based on As. Anal. Calcd (found) for **3**·4H$_2$O ($C_{34}H_{70}Fe_3As_8N_3O_{25}$): C: 24.19 (23.79); H: 4.18 (4.18); N: 2.49

https://dx.doi.org/10.1021/acs.inorgchem.0c02554
Inorg. Chem. 2020, 59, 18090−18101

(2.56). Selected IR data (KBr disk, cm^{-1}): 501(w), 609(w), 646(w), 863(vs), 1112(m), 1383(s), 1465(s), 1497(s), 3406(br).

X-ray Crystallography. X-ray data for **1**·15MeCN, **2**·2MeCN·$2H_2O$, and **3**·4MeOH were collected at 100 K on a Bruker DUO diffractometer using MoKα radiation (λ = 0.71073 Å) and an APEXII CCD area detector. Raw data frames were read by program SAINT and integrated using 3D profiling algorithms.[37] The resulting data were reduced to produce *hkl* reflections and their intensities and estimated standard deviations. The data were corrected for Lorentz and polarization effects, and numerical absorption corrections were applied based on indexed and measured faces. The structures were solved and refined in *SHELXTL2014*, using full-matrix least-squares refinement cycles.[38] These were carried out by minimizing the wR_2 function using F^2 rather than F values. R_1 is calculated to provide a reference to the conventional R value, but its function is not minimized. The non-H atoms were refined with anisotropic thermal parameters, and all the H atoms were calculated in idealized positions and refined as riding on their parent atoms. All crystal data and refinement details are collected in Table 1.

For **1**·15MeCN, the asymmetric unit consists of a complete Fe_{12} cluster cation, three Cl^- counterions, and ~15 MeCN solvent molecules, most of which were disordered and could not be modeled properly. Thus, program SQUEEZE,[39] a part of the PLATON package of crystallographic software, was used to calculate the solvent disorder area and remove its contribution to the overall intensity data. One $Me_2AsO_2^-$ ligand was disordered about two positions that refined with 50:50% occupancies. In the final cycle of refinement, 30663 reflections (of which 20353 are observed with $I > 2\sigma(I)$) were used to refine 1461 parameters, and the resulting R_1, wR_2, and S (goodness of fit) were 7.22%, 16.69%, and 1.023, respectively.

For **2**·2MeCN·$2H_2O$, the asymmetric unit contains half the $Fe_{12}Na_2$ cluster cation lying on an inversion center, two half-occupancy Na^+ ions, three NO_3^- ions, and one MeCN and one H_2O solvent molecules. Two arsinate ligands exhibit some slight disorder and were refined in two parts, and the three NO_3^- counterions showed slight rotational disorder. There was extensive hydrogen bonding between the various cations and anions. In the final cycle of refinement, 28930 reflections (of which 23228 are observed with $I > 2\sigma(I)$) were used to refine 851 parameters, and the resulting R_1, wR_2, and S (goodness of fit) were 4.24%, 8.79%, and 1.085, respectively.

For **3**·4MeOH, the asymmetric unit consists of a half Fe_3 complex lying on an inversion center, a half-occupancy NO_3^- counterion, and two MeOH solvent molecules. The latter were badly disordered over four positions and could not be modeled properly, and thus, program SQUEEZE was again used to remove their intensity contributions.[39] One arsinate ligand (As2) is disordered and was refined in two positions with 93:7% occupancies. The H atom on unbound O3 of the arsinic acid ligand was obtained from a difference Fourier map and refined freely. The half nitrate counterion is located on an inversion center and disordered so that an O atom shares the same position as the second nitrate nitrogen position. In the final cycle of refinement, 7736 reflections (of which 6440 are observed with $I > 2\sigma(I)$) were used to refine 324 parameters, and the resulting R_1, wR_2, and S (goodness of fit) were 3.77%, 7.63%, and 1.045, respectively.

DFT Calculations. To make DFT calculations for **1** computationally tractable, we considered one Fe_6 half of the full Fe_{12} structure taken from the CIF data by cleaning extraneous atoms, i.e., minor ligand disorder positions, Cl^- counterions, and lattice solvent. This simplification leads to a total of 15 distinct J_{ij} exchange couplings and 32 Ising-type spin vector configurations: 1 high spin, 6 with one spin inversion, 15 with two spin inversions, and 10 with three spin inversions. The energies of these configurations can be expressed in terms of a sum over all spin interactions (eq 1) where $\langle ij \rangle$ stands for all *ij* pairs, $S_k = \pm^5/_2$ for Fe^{III}, and E_0 is a constant that serves to equate

$$E(\{S\}) = -2\sum_{\langle ij \rangle} J_{ij} S_i \cdot S_j + E_0 \quad (1)$$

the spin model and DFT energies. To determine the exchange couplings, the energies of all 32 configurations were evaluated from broken spin-symmetry DFT calculations, and the resulting energies were used to perform a linear fit of the Ising-type energy expression in eq 1. This strategy has been successfully used in the literature to extract exchange couplings in multicenter transition metal complexes.[40−44] The R^2 for the linear regression differs from unity by less than 10^{-7}, which indicates that the magnetization is tightly localized at the magnetic centers, and thus, the DFT calculations behave energetically like an Ising system. We have also verified that the atomic spin populations obtained are consistent with the expected broken spin symmetry configuration.

DFT calculations were performed using the hybrid version of the Perdew−Burke−Ernzerhof (PBEh) functional, which incorporates 25% of exact (Hartree−Fock-type) exchange. This functional is known to perform well for magnetic exchange couplings[45] and for the particular case of oxo-bridged Fe··Fe couplings to yield an RMS error of ~10%, as shown for a set of 11 dinuclear Fe^{III} complexes.[46] Pople's 6-311+G** basis was used for Fe atoms and the 6-31G** for lighter elements.[47,48] All calculations included all the electrons and neglected scalar and spin−orbit relativistic effects. All calculations were performed using an in-house version of the Gaussian 16 program[49] that allows for a simple spin inversion of the magnetic centers to produce a reasonable initial guess for self-consistent calculations. No symmetry was assumed at any point in the model or the DFT calculations. A self-consistency convergence threshold of 10^{-6} Ha = 0.2 cm^{-1} in the energy and 10^{-8} in the RMS changes in the density matrix was used in all calculations.

Other Studies. Infrared spectra were collected in the solid state (KBr pellets) in the 400−4000 cm^{-1} range using a Nicolet Nexus 670 FTIR spectrometer. Direct current (dc) and alternating current (ac) magnetic susceptibility measurements were performed on vacuum-dried polycrystalline solids, embedded in eicosane to prevent torquing, with a Quantum Design MPMS-XL SQUID magnetometer capable of operating with applied dc fields up to 7 T in the 1.8−400 K range. dc studies were carried out in the 5.0−300.0 K range in a 0.1T (1000 Oe) magnetic field, and ac studies were carried out in the 1.8−15.0 K range in an ac field of 3.5 G and oscillation frequencies up to 1500 Hz. Program PHI[50] was used for fitting the dc susceptibility data. Fits to the Van Vleck equation were performed using the program Sigmaplot. Elemental analyses (C, H, N) were performed on vacuum-dried samples at Atlantic Microlab, Inc.

RESULTS AND DISCUSSION

Syntheses. The pK_a values of some carboxylic and pseudocarboxylic acids are compared in Table 2, and

Table 2. pK_a of Common Carboxylic and Some Pseudocarboxylic Acids

acid	pK_a	ref
acetic acid ($MeCO_2H$)	4.76	24
benzoic acid ($PhCO_2H$)	4.20	24
pivalic acid ($^tBuCO_2H$)	5.03	24
diphenylphosphinic acid (Ph_2PO_2H)	2.32	25
benzenesulfonic acid ($PhSO_3H$)	−2.80	26
dimethylarsinic acid (Me_2AsO_2H)	6.27	27

Me_2AsO_2H can be seen to be significantly less acidic than even pivalic acid. Thus, its conjugate base should be a strong donor ligand, but the high pK_a suggested that carboxylate substitution by Me_2AsO_2H in a preformed cluster might not be the best reaction strategy. Nevertheless, since many synthetic routes to high nuclearity Fe/O/RCO_2^- clusters have employed the common $[Fe_3(O_2CR)_6(H_2O)_3]^+$ salts as preformed starting materials, we decided for comparative reasons to initiate our studies using the analogous reaction system with arsinic acid but employing the R = ^{t}Bu derivative to facilitate carboxylate protonation and replacement as pivalic acid, and

https://dx.doi.org/10.1021/acs.inorgchem.0c02554
Inorg. Chem. 2020, 59, 18090−18101

this proved successful. Thus, the Fe_3:Me_2AsO_2H reaction in a 1:4 ratio gave $[Fe_{12}O_4(O_2C^tBu)_8(O_2AsMe_2)_{17}(H_2O)_3]Cl_3$ (**1**) in ~30% yield (eq 2). Since Me_2AsO_2H is the

$$4[Fe_3O(O_2CR)_6(H_2O)_3]^+ + 17Me_2AsO_2H \rightarrow [Fe_{12}O_4(O_2CR)_8(O_2AsMe_2)_{17}(H_2O)_3]^{3+} + H^+ + 9H_2O + 16RCO_2H \quad (2)$$

limiting reagent, we explored the 1:4.25 reaction, as well as 1:6 and 1:8 but obtained the same product **1** in comparable yield in each case. Decreasing the ratio to 1:3 also gave **1** but in a lower yield of 15%. Adding NEt_3 gave a mixture of **1** and other products (as judged by IR spectra) that we could not separate. Use of the R = Me starting material gave the corresponding product to **1**, as judged by IR spectral comparison (Figure S1), and it was not studied further.

To exclude carboxylates completely, reactions of simple Fe^{III} salts with NaO_2AsMe_2 were investigated, and this led to **2**, a salt of another Fe_{12} cluster (eq 3) with some structural similarity to **1** (vide infra). Small changes to the Fe:$Me_2AsO_2^-$ ratio did not affect the product or its yield.

$$12Fe(NO_3)_3 + 22NaO_2AsMe_2 + 10H_2O \rightarrow [Fe_{12}Na_2O_4(O_2AsMe_2)_{20}(Me_2AsO_2H)_2(H_2O)_6(NO_3)_6]^{4+} + 20NaNO_3 + 6HNO_3 + 4NO_3^- \quad (3)$$

We recently reported the synthesis of two Fe/O/RCO_2^-/hqn^- clusters of nuclearity Fe_6 and Fe_8 from the reaction of $[Fe_3O(O_2CR)_6(H_2O)_3]^+$ with 8-hydroxyquinoline (hqnH).[2] Thus, for comparison we have explored similar reactions using Me_2AsO_2H and found that the Fe^{3+}/Me_2AsO_2H/hqnH/NEt_3 = 1:2.5:0.7:3 ratio leads to the $[Fe_3(O_2AsMe_2)_6(hqn)_2(Me_2AsO_2H)_2]^+$ cation of **3** (eq 4). Not only is this completely different from the hqnH products with carboxylates, it is also extremely unusual in containing no monatomic O^{2-}, HO^-, RO^-, or related group bridging

$$3Fe^{3+} + 8Me_2AsO_2H + 2hqnH + 8NEt_3 \rightarrow [Fe_3(O_2AsMe_2)_6(Me_2AsO_2H)_2(hqn)_2]^+ + 8NHEt_3^+ \quad (4)$$

Fe_2 pairs (vide infra). The MeOH assisted solubility of all reagents, and no product was isolated if NEt_3 was not added. The indicated reagent ratio was the one that gave the highest yield of pure material.

Description of Structures. **1**·15MeCN crystallizes in monoclinic space group $P2_1/c$ with the Fe_{12} cation in a general position. The complete structure of the cation and its partially labeled core are shown in Figure 1, and selected bond distances and angles are listed in Table S1. The structure comprises four triangular $\{Fe^{III}_3(\mu_3\text{-}O^{2-})\}$ units, as found in the starting material, linked in pairs by two $\eta^2{:}\eta^1{:}\mu_3$ and one $\eta^2{:}\eta^2{:}\mu_4$ $Me_2AsO_2^-$ groups each (Scheme 1) into two intimately connected Fe_6 subunits (Fe3··Fe4 = 3.272(3) Å; Fe9··Fe10 = 3.273(3) Å). These are then linked by two *anti*–*anti* $\eta^1{:}\eta^1{:}\mu$ $Me_2AsO_2^-$ groups (Fe1··Fe12 = 6.462(3) Å; Fe6··Fe7 = 6.495(3) Å) into the complete Fe_{12} core with a rectangular looplike structure. Each Fe_3 triangle is isosceles, with one edge monoatomically bridged by two O atoms. Peripheral ligation is completed by eight $^tBuCO_2^-$ and eight $Me_2AsO_2^-$ groups all in the common *syn*–*syn* $\eta^1{:}\eta^1{:}\mu$ bridging mode, a terminal H_2O ligand on Fe2/Fe8/Fe11 atoms at three corners of the structure, and a terminal monodentate $Me_2AsO_2^-$ on Fe5 at the fourth corner. If the latter difference is ignored, then the cluster has virtual C_{2h} symmetry, with the C_2 axis passing through the midpoints of the Fe3–Fe4 and Fe9–Fe10 vectors and can be described as a dimer of Fe_6 units. Fe and As oxidation states and O protonation levels were confirmed by BVS calculations (Table S2).[51] There is a pair of

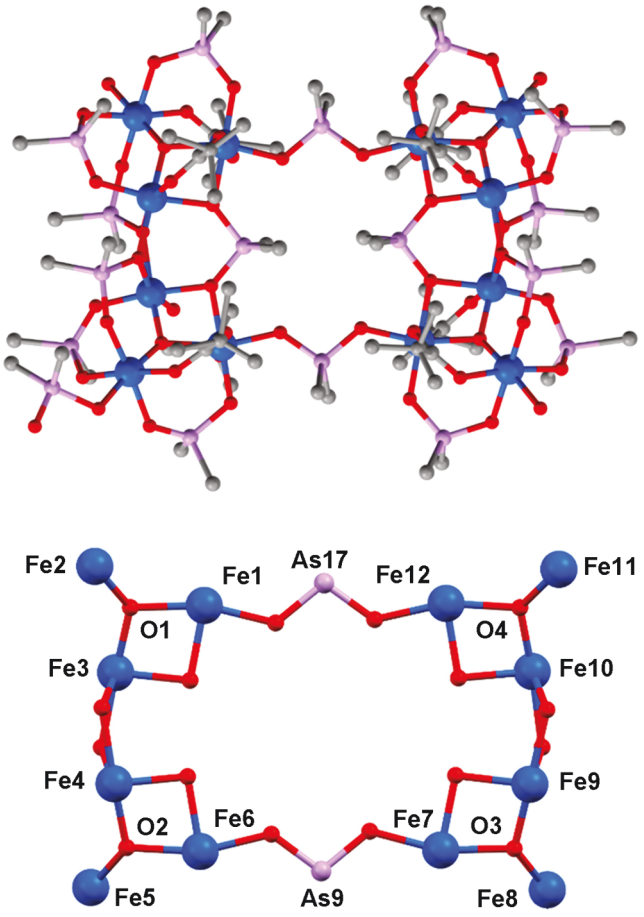

Figure 1. (top) Complete structure of the cation of **1**, with H atoms removed for clarity, and (bottom) its Fe–oxo core; O1–4 are O^{2-} ions, and the other O atoms are all from $Me_2AsO_2^-$ groups. Color code: Fe blue; As violet; O red, C gray.

Scheme 1. Carboxylate and Arsinate Bridging Modes Found in Complexes 1–3

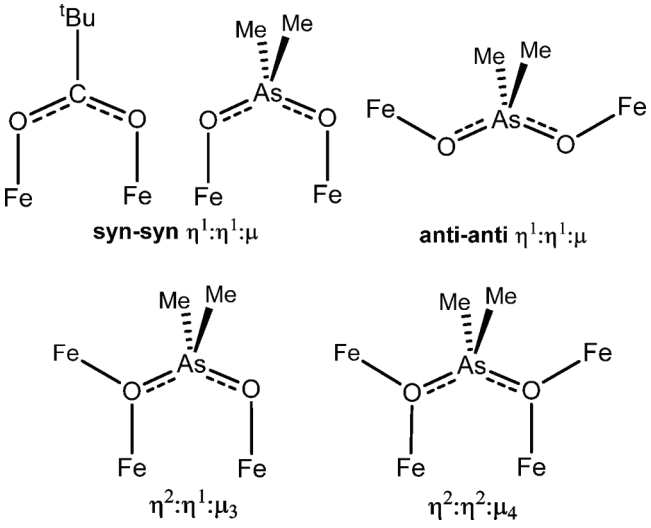

https://dx.doi.org/10.1021/acs.inorgchem.0c02554
Inorg. Chem. 2020, 59, 18090–18101

adjacent O−H···O hydrogen bonds at each end of the Fe_{12} cations directly to neighboring cations that lead to H-bonded chains. These each involve a terminal H_2O (O55, O56) ligand on Fe2 and Fe8 of neighboring cations and a nearby $Me_2AsO_2^-$ O atom (O7, O24) on the neighbor (O7···O56 = 2.821(12)Å, O24···O55 = 2.633(12) Å) (Figure S2). The structure of **1** is somewhat reminiscent of that reported previously for $[Mn_{16}X_4O_8(O_2CPh)_{16}(Me_2AsO_2)_{24}]$ (X = Ca^{2+} or Sr^{2+}), which can be similarly described as a dimer since it comprises two $Mn_{10}X_4$ units held together into a loop structure by two *anti*−*anti* $\eta^1{:}\eta^1{:}\mu$ $Me_2AsO_2^-$ groups and with each unit containing a central $\eta^2{:}\eta^2{:}\mu_4$ $Me_2AsO_2^-$ group as in **3** (Figure S3).[17]

2·2MeCN·2H_2O crystallizes in space group $P2_1/c$ with the $Fe_{12}Na_2$ cation lying on an inversion center. Its complete structure and a partially labeled Fe_6 core are shown in Figure 2,

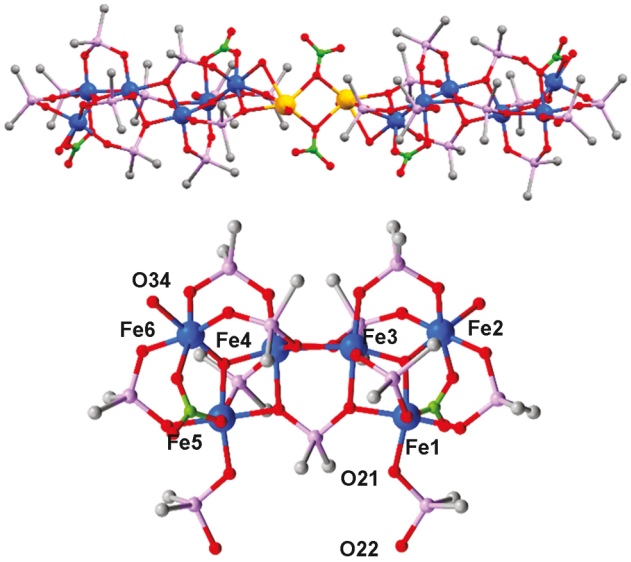

Figure 2. (top) Complete structure of the centrosymmetric $Fe_{12}Na_2$ cation of **2**, from a viewpoint that emphasizes the two $\eta^2{:}\eta^1{:}\mu_3$ $Me_2AsO_2^-$ groups in each Fe_6 unit and the $\{Na_2(NO_3)_2\}$ central bridging unit. H atoms have been removed for clarity. (bottom) One Fe_6 unit from a viewpoint emphasizing its $\eta^2{:}\eta^2{:}\mu_4$ $Me_2AsO_2^-$ group. Color code: Fe blue; Na gold, As violet; O red, N green, C gray.

and selected bond distances and angles are listed in Table S3. The structure can again be described as a dimer of two Fe^{III}_6 units, with the cores of the latter being very similar to those in **1**, i.e., two isosceles Fe_3 units bridged by two $\eta^2{:}\eta^1{:}\mu_3$ and one $\eta^2{:}\eta^2{:}\mu_4$ $Me_2AsO_2^-$ groups. The main differences are (i) the four *syn*−*syn* $\eta^1{:}\eta^1{:}\mu$ $^tBuCO_2^-$ ligands of **1** have been replaced by two $Me_2AsO_2^-$ and two NO_3^- groups bridging like the carboxylates, and (ii) the two Fe_6 units are bridged into a linear structure by a central $\{Na_2(\mu\text{-}NO_3)_2\}$unit. As a result, the two *anti*−*anti* $\eta^1{:}\eta^1{:}\mu$ $Me_2AsO_2^-$ that formed the dimer in **1** are now monodentate terminal ligands in **2**, with one of them protonated (O22) as confirmed by O BVS (Table S4) but both still using an *anti* lone pair to do so. Two Na^+ and six NO_3^- counterions complete the double-salt compound.

In order to quantitatively compare the Fe_6 cores of **1** and **2**, root-mean-square deviation (RMSD) calculations were carried out.[52] The result (Figure S4) gives a weighted RMSD for the whole Fe_6 unit of only 0.107 Å. Deviations for the Fe atoms are within 0.1 Å except for Fe2 and Fe4 (0.126 and 0.174 Å, respectively) probably because at these atoms pivalate ligands in **1** are replaced by NO_3^- ligands in **2**. These deviations notwithstanding, the Fe_6 units of **1** and **2** are essentially isostructural. Therefore, we conclude this Fe_6 unit to be a favored structural unit in Fe/O/$Me_2AsO_2^-$ chemistry, even with some carboxylate incorporation. Within Fe/O/RCO_2^- cluster chemistry there are a number of Fe_6 topologies, many of them comprising linked triangular units with "chairlike", "planar", "twisted-boat", stacked triangles, linked triangles, octahedral, and fused or extended butterflies,[53−58] but nevertheless, none of them are the same as the Fe_6 unit of **1** and **2**, most likely due to the $\eta^2{:}\eta^2{:}\mu_4$ $Me_2AsO_2^-$ binding mode that supports it, which is unknown in Fe^{III} carboxylate chemistry (vide infra).

3·4MeOH crystallizes in the monoclinic space group $C2/c$ with the Fe_3 cation lying on an inversion center. Its partially labeled structure is shown in Figure 3, and selected bond

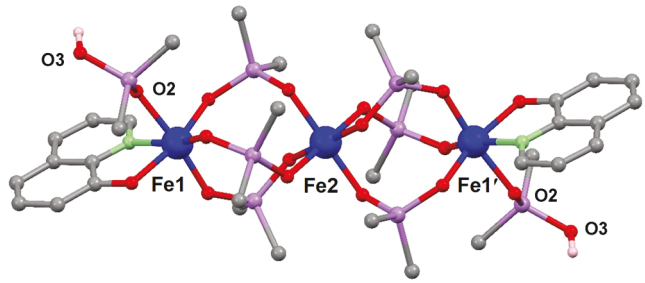

Figure 3. Structure of the centrosymmetric Fe_3 cation of **3**, with H atoms removed for clarity except those on the monodentate Me_2AsO_2H ligands. Color code: Fe blue; As violet; O red, N green, C gray, H pink.

distances and angles are listed in Table S5. The structure consists of a linear Fe^{III}_3 unit with each Fe_2 pair bridged by three *syn*−*syn* $\eta^1{:}\eta^1{:}\mu$ $Me_2AsO_2^-$ groups. There are no monatomic bridges, and thus, the Fe···Fe separations are long (4.585(1) Å). The Fe−O−As−O−Fe bridges are more distorted than those in **1** and **2**: For *syn*−*syn* $\eta^1{:}\eta^1{:}\mu$ Fe−O−As−O−Fe bridges in **1**, the torsion angles between the two Fe−O are ∼10°, but those in **3** are ∼70°. Ligation is completed by a chelating hqn^- and a monodentate Me_2AsO_2H on each outer Fe; Fe oxidation states and O protonation levels were determined by BVS calculations (Table S6). There are two intermolecular O−H···O hydrogen bonds at each end of the Fe_3 cations linking them into linear chains that all run parallel in the crystal. These involve the protonated O3 of the Me_2AsO_2H ligand and the bound O2 of the same ligand on the neighboring cation (O2···O3 = 2.638(4) Å).

Comparison of Dimethylarsinate and Carboxylate Chemistry. Although the number of Fe/O/arsinate compounds is still small, it is nevertheless instructive to compare them with Fe/O/carboxylate chemistry. Two major points can be noted: (**i**) Carboxylates can also display different bridging modes in Fe/O chemistry and elsewhere, but $Me_2AsO_2^-$ appears to more readily employ its *anti* lone pairs and give μ_3- and μ_4-bridging modes, as well as the *anti*−*anti* μ_2 mode that is rare for carboxylates. All three bridging modes are found in **1** and **2** and also the related $[Mn_{16}X_4O_8(O_2CPh)_{16}(O_2AsMe_2)_{24}]$ (Figure S3). The $\eta^2{:}\eta^2{:}\mu_4$ mode is also very rare for carboxylates—it is found, for example, in the $[Ce_3Mn_8O_8(RCO_2)_{18}(RCO_2H)_2]$ clusters,[59] but we are unaware of an example in Fe^{III} chemistry. (**ii**) The absence of a monoatomi-

https://dx.doi.org/10.1021/acs.inorgchem.0c02554
Inorg. Chem. 2020, 59, 18090−18101

cally bridging O^{2-}, HO^-, or RO^- (R = alkyl or aryl) group in **3** is extremely rare in Fe^{III} carboxylate chemistry.[60,61] Even in Fe^{II} chemistry such bridges are often to be found, typically from carboxylate O atoms.[62,63]

The most plausible explanation is the higher basicity of $Me_2AsO_2^-$, as reflected in the pK_a of the acid. For carboxylates, the *syn* O lone pairs are recognized, both experimentally and computationally, to be more basic than the *anti* pairs, leading to predominant *syn*−*syn* carboxylate bridging.[64,65] Thus, when the *anti* lone pairs do get involved, it is often in addition to the *syn* ones, and this is certainly true for Fe^{III}.[66] Indeed, at one time all known Fe^{III} carboxylate complexes had the *syn* binding mode,[67] and although there are now examples using *anti* lone pairs,[68,69] the *syn*−*syn* binding mode is still by far the majority.

The greater basicity of dimethylarsinate will make both the *syn* and *anti* lone pairs better donor groups and rationalize the variety of bridging modes seen even in the few clusters prepared to date. The high basicity likely also rationalizes the absence of Fe−O−Fe bridges in **3** by mollifying the metal's charge density without recourse to hard oxide or similar ions. In **1**, another reason why arsinate groups link the two Fe_6 units rather than carboxylates is steric hindrance: the space-filling diagram (Figure S5) shows that the Me groups of the two $\eta^2{:}\eta^2{:}\mu_4$ groups are already in close contact, and given that the arsinate O···O distance is 0.5−0.6 Å longer than that for a carboxylate in the equivalent binding mode, we estimate that linkage of the two Fe_6 units by $\eta^2{:}\eta^2{:}\mu_4$ carboxylates would require them to be ∼0.4 Å closer together, which is clearly not possible on steric grounds.

Relevance to Environmental Studies. As mentioned in the Introduction, there have been several studies of the surface interactions of iron oxides and dimethylarsinic acid. For example, by analyzing the absorption of the acid on goethite (an iron(III) oxide-hydroxide) with X-ray absorption spectroscopy, Shimizu et al. concluded an Fe··As distance of ∼3.3 Å and ∼1.8 Fe per As atom, which matches well with those for Fe_2 units bridged by *syn*−*syn* $\eta^1{:}\eta^1{:}\mu$ arsinates in **1** and **2** (3.19−3.31 Å).[31] Additional studies by Nguema et al. were in agreement.[32] The μ_3- and μ_4-modes in **1** and **2** have longer Fe·· As distances (typically 3.4−3.5 Å) and should provide a useful distinction for identifying other interactions between dimethylarsinic acid and iron oxide-based minerals.

Magnetic Susceptibility Studies. Variable-temperature dc magnetic susceptibility (χ_M) data were collected on crushed vacuum-dried microcrystalline samples in the 5.0−300 K range in a 0.1 T (1 kG) applied dc field and are plotted as $\chi_M T$ vs T.

For **1**, $\chi_M T$ decreases steadily from 18.8 cm^3 K mol^{-1} at 300 K to 0.80 cm^3 K mol^{-1} at 5.0 K (Figure 4). The 300 K value is much lower than that for 12 noninteracting high-spin Fe^{III} ions with g = 2 (52.5 cm^3 K mol^{-1}) indicating dominant antiferromagnetic (**AF**) interactions in **1**, and the 5.0 K value indicates an S = 0 ground state. For **2**, a similar profile is seen, with $\chi_M T$ decreasing steadily from 20.8 cm^3 K mol^{-1} at 300 K to 2.43 cm^3 K mol^{-1} at 5.0 K (Figure 4), again indicating dominant **AF** interactions and an S = 0 ground state.

We realized that with 12 Fe^{III} ions in **1** and **2**, low crystallographic symmetry, and a large number of inequivalent J_{ij} Fe_2 pairwise exchange interactions, it would be very difficult to get meaningful fits of the data. On the basis of prior experience, we thus took the following steps: (i) since **1** and **2** are both Fe_6 dimers bridged by units that should give at best weak exchange interactions, the two Fe_6 units were assumed to be noninteracting, and the fits thus performed on $\chi_M T$ per Fe_6 unit; and (ii) the C_2 virtual symmetry of each Fe_6 unit was applied. As a result, the system reduces to a 4-J model (Scheme 2). However, as we have shown elsewhere,[2] even a 4-J fit can give many excellent but very different fits depending on the input values. As a test, we fit the data for **1**, divided by two to make it per Fe_6 unit, with three reasonable sets of input values, namely 0, −10, and −20 cm^{-1}, and got excellent fits in each case but with very different fit parameters (Table 3); however, none of these were acceptable based on expected values for the Fe_2 structural units—and multiple runs for given inputs did not always give the same best fit! In particular, J_{13} is much too

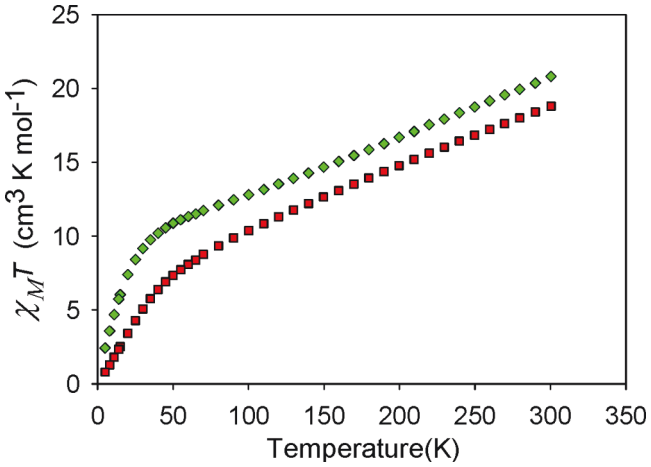

Figure 4. $\chi_M T$ vs T per Fe_{12} for **1** (red) and **2** (green).

Scheme 2. Exchange Coupling Model Used for 1 and 2

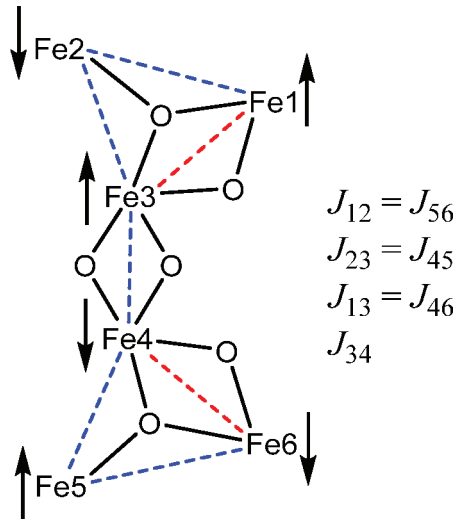

Table 3. Typical Fits of $\chi_M T$ vs T Data for 1 with Different Input Values

J^a	Fit(0)^{b,c}	Fit(−10)^{b,c}	Fit(−20)^{b,c}
J_{12}	−35.6	−37.5	−15.2
J_{23}	−25.0	−11.6	−32.7
J_{13}	−29.5	−26.0	−32.7
J_{34}	+35.6	−5.7	−9.7

[a]Using the atom labeling in Scheme 2. [b]cm^{-1}; $\hat{H} = -2J_{ij}\hat{S}_i \cdot \hat{S}_j$ convention. [c]Fit(n) are fit values using input J_{ij} of n cm^{-1}.

https://dx.doi.org/10.1021/acs.inorgchem.0c02554
Inorg. Chem. 2020, 59, 18090−18101

strong for a bis-monoatomically bridged {Fe(O)$_2$Fe} unit, which almost always has a J in single figures, and the strong ferromagnetic (**FM**) J_{34} is completely unrealistic for such Fe$^{III}_2$ units.

Using the protocol described elsewhere, we therefore sought good estimates of the J values to use as input values to get more reliable fits with J's closer to "reality". This was achieved by two independent approaches, namely DFT calculations and the magnetostructural correlation (MSC) developed specifically for use with high nuclearity Fe^{III} clusters,[2] since we found previously that those available for dinuclear Fe$^{III}_2$ compounds are unreliable for higher nuclearities.[2] The DFT calculations used a broken-symmetry approach on one Fe$_6$ unit yielding 32 distinct Ising-type spin vector configurations and 15 J_{ij} exchange couplings (see the Experimental Section), of which seven are nearest-neighbor couplings and the rest are non-nearest-neighbor. The obtained values (Table 4) are in the expected range, with the mono-oxo-bridged Fe$_2$ pairs having stronger antiferromagnetic (**AF**) interactions than the bis-oxo {Fe(O)$_2$Fe} pairs, consistent with the larger Fe−O−Fe angles in the former. No virtual symmetry was assumed, but we still see three pairs of similar couplings that validate the assumption of imposing C_2 virtual symmetry on the Fe$_6$ core used in the MSC model and fits (vide infra).

Table 4. DFT Calculated J_{ij} Values for One Fe$_6$ Unit of 1

J_{ij}[a]	J[b]	J_{ij}[a]	J[b]
J_{12}	−28.2	J_{56}	−26.8
J_{23}	−34.3	J_{45}	−33.1
J_{13}	−7.3	J_{46}	−8.6
J_{34}	−3.6	J_{16}	−1.6
J_{35}	−0.4	J_{36}	+0.1

[a]Using the atom labeling in Scheme 2. [b]cm^{-1}; $\hat{H} = -2J_{ij}\hat{S}_I\cdot\hat{S}_j$ convention.

The MSC calculations were based on the expression in eq 5 developed by Mitchell et al.[2]

$$J_{ij} = (1.23 \times 10^9)(-0.12 + 1.57\cos\varphi + \cos^2\varphi)e^{-8.99r} \quad (5)$$

where r is the average Fe−O bond length, and φ is the Fe−O−Fe bond angle, further averaged under the virtual symmetry described above. This model, based on the one developed by Weihe et al. for dinuclear Fe$^{III}_2$ compounds using the angular overlap model,[70] has been previously applied to many carboxylate-containing Fe^{III}−oxo clusters and proven very successful, but this was its first use for arsinate-ligated clusters. The Fe−O and Fe−O−Fe values for **1**, the resulting J_{MSC}, and the J_{DFT} (all averaged to C_2 virtual symmetry) are collected in Table 5, where it can be seen that the J_{MSC} and J_{DFT} are in reasonable agreement and as expected for mono- vs bis-oxo-bridged Fe$_2$ pairs.

The J_{MSC} and J_{DFT} can now be used to rationalize the ground state of the Fe$_6$ unit of **1**. The J_{ij} values separate into strong (J_{12}, J_{23}) and weak (J_{13}, J_{34}), with the Fe$_3$ triangles at each end containing two of the former and one of the latter. Spin frustration (competing exchange interactions) will thus occur in these triangles, and the two strong will clearly dominate giving the spin vector alignments in Scheme 2. The weak interactions are **AF**, but they are frustrated (shown in red); and the spins are forced to align parallel by the stronger interactions, a situation we have encountered on a number of occasions.[2,3] Each triangle thus has $S = {}^5/_2$, and they align antiparallel due to **AF** J_{34}, which is very weak but not competing with another interaction; and thus, the overall spin of the Fe$_6$ unit is $S = 0$. The value of J_{16}, the long-distance coupling of Fe1/Fe6 by the *anti* lone pairs of the $\eta^2{:}\eta^2{:}\mu_4$ arsinate, also suggests the coupling between the two Fe$_6$ units to be comparable and supports the approximation to treat the Fe$_6$ halves as magnetically independent units. The overall ground state of **1** is thus $S = 0$, as found experimentally. The same arguments also apply to **2**, rationalizing its overall $S = 0$ ground state.

Table 5. Fits of $\chi_M T$ vs T Data with Different Input Values for 1 and 2

	J[a]	Fe−O (av, Å)	Fe−O−Fe (av, deg)	J_{MSC}[b]	J_{DFT}[b]	J_{PHI}[b]
1	J_{12}	1.939	119.8	−21.6	−27.5	−37.5(1)
	J_{23}	1.913	132.3	−30.3	−33.7	−25.9(9)
	J_{13}	1.998	99.0	−6.6	−8.0	−11.6(4)
	J_{34}	2.101	102.4	−3.2	−3.6	−5.7 (4)
2	J_{12}	1.900	125.4	−30.2		−33.5(3)
	J_{23}	1.904	124.3	−28.6		−19.8(6)
	J_{13}	2.016	100.5	−5.9		−10.9(4)
	J_{34}	2.059	103.2	−4.5		−1.9(5)

[a]Using the atom labeling in Scheme 2. [b]cm^{-1}; $\hat{H} = -2J_{ij}\hat{S}_I\cdot\hat{S}_j$ convention.

The J_{MSC} and J_{DFT} for **1** were used as inputs to fit the experimental data with PHI (Figure 5a).[50] First, we simulated the $\chi_M T$ vs T plot using the J_{MSC} values (black dashed line) and J_{DFT} values (red dashed line); they reproduced the general profile of the experimental data but with significant discrepancy. A satisfactory fit was then obtained (solid red line) with the parameters in Table 5, and temperature-independent paramagnetism (TIP) held constant at 600 × 10^{-6} cm^3 mol^{-1}.[2] We found the same fit starting with the J_{MSC} or J_{DFT} as inputs, and the same fits were obtained each time the procedure was run. For **2**, the simulation using J_{MSC} values gave a good agreement with the experimental data (dashed line in Figure 5b) and a subsequent excellent fit (green line) with the parameter values in Table 5. Finally, to complement the dc studies and to preclude any complicating effect of the dc field on the lowest T data, ac in-phase susceptibility data for **1** and **2** were collected (Figure S6) and show a faster increase with increasing T for **2** vs **1**, consistent with a weaker J_{34} for the former vs the latter, as found in the fit, and thus lower-lying excited states in **2** vs **1**. The latter is also seen in the calculated spin energy plots (Figure S7).

For **3**·4H$_2$O, $\chi_M T$ is 12.9 cm^3 K mol^{-1} at 300 K and remains almost constant with decreasing temperature to ∼100 K and then decreases more rapidly to 4.79 at 5.0 K (Figure 6a). The 300 K value is close to that for three noninteracting Fe^{III} ions with $g = 2$ (13.1 cm^3 K mol^{-1}); this and the plot profile indicate very weak **AF** interactions, and the 5.0 K value suggests an $S = {}^5/_2$ ground state. There are no Fe−O−Fe bridges in **3** so the MSC is not applicable, but this is a 2-J system that can readily be fit by PHI or the appropriate Van Vleck equation to the model in Figure 6a (inset).

The appropriate spin Hamiltonian is given by eq 6, where $J_{12} = J_{1'2}$ due to the inversion center

$$H = -2J_{12}(\hat{S}_1\cdot\hat{S}_2 + \hat{S}_{1'}\cdot\hat{S}_2) - 2J_{11'}(\hat{S}_1\cdot\hat{S}_{1'}) \quad (6)$$

https://dx.doi.org/10.1021/acs.inorgchem.0c02554
Inorg. Chem. 2020, 59, 18090−18101

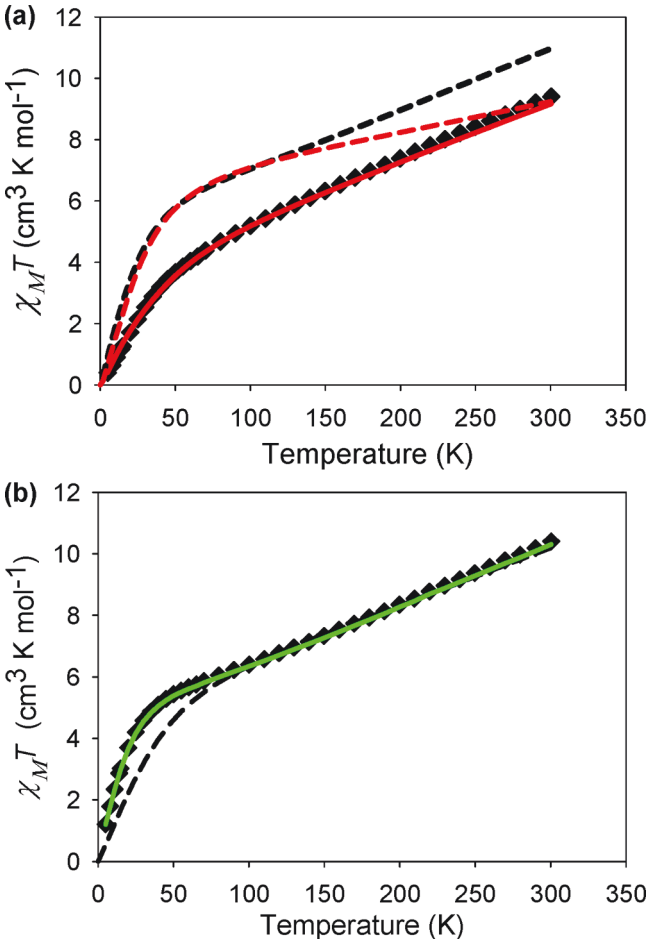

Figure 5. $\chi_M T$ vs T data per Fe_6 for (a) **1** and (b) **2**. The dashed lines are simulations using the J_{MSC} values, and the colored lines are fits to the 4-J model in Scheme 2. See Table 5 for the fit parameters.

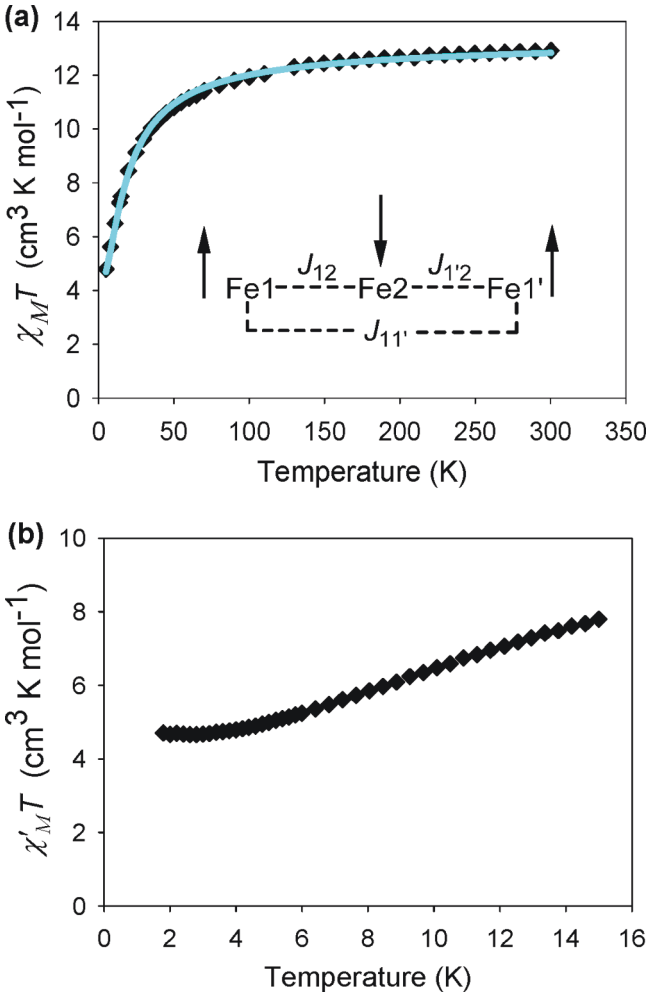

Figure 6. (a) $\chi_M T$ vs T for **3**. The solid line is the fit to the 2-J model in the inset with $J_{11'} = 0$ and $g = 2.0$. See Table 6 for the fit parameters. (b) In phase ac, $\chi'_M T$ vs T for **3** confirming an $S = {}^5/_2$ ground state.

and is the same as that for an isosceles triangle.[71,72] The overall spin state energies, $E(S_T)$, are given by eq 7, where $\hat{S}_A = \hat{S}_1 + \hat{S}_{1'}$, and $\hat{S}_T = \hat{S}_A + \hat{S}_2$.[73] Fits of the data to the Van Vleck equation or by

$$E(S_T) = -J_{12}[S_T(S_T + 1) - S_A(S_A + 1)] - J_{11'}[S_A(S_A + 1)] \quad (7)$$

PHI gave J_{VV} and J_{PHI} with identical values of J_{12} (Table 6) and a very small $J_{11'}$ with large uncertainties; we thus used both a fixed $J_{11'} = 0$ and $g = 2$, and this gave $J_{PHI} = J_{12} = -0.80(1)$ cm^{-1} with a constant TIP = 300×10^{-6} cm^3 mol^{-1} (solid line in Figure 6a). A DFT calculation led to the same conclusion of a weakly coupled system, giving $J_{12} = -0.8$ cm^{-1}, $J_{11'} = 0$, and $g = 2.0$. The very weak J_{12} is consistent with the structure of **3** and the absence of monatomic bridging, and its **AF** nature suggests an $S = {}^5/_2$ ground state from the spin vector ordering of Figure 6a (inset). The weak J_{12} also validates our assumption in the analyses for **1** and **2** that the primary exchange coupling pathway is through the Fe−O−Fe units with only minor contributions from the arsinate ligands and that both compounds could be analyzed as two essentially noninteracting Fe_6 units.

Again to preclude any complicating effect of the dc field on the data of such a weakly coupled system as **3** and to confirm its ground state, ac data were collected and plotted as $\chi'_M T$ vs T (Figure 6b). The decreasing $\chi'_M T$ is consistent with low-lying excited states, as expected for a weakly coupled **AF** system, and it reaches a plateau of ∼4.4 cm^3 K mol^{-1} at ∼3 K, confirming an $S = {}^5/_2$ ground state; spin-only $\chi'_M T$ for $S = {}^3/_2$, ${}^5/_2$, and ${}^7/_2$ is 1.88, 4.38, and 7.88 cm^3 K mol^{-1}, respectively.

Table 6. Exchange Couplings in 3 from Fits of Experimental Data and DFT

parameter	J_{VV}[a,b]	J_{PHI}[a,c]	J_{PHI}[a,d]	J_{DFT}[a]
$J_{12}/J_{1'2}$	−0.83(3)	−0.83(2)	−0.80(1)	−0.8
$J_{11'}$	0.038(74)	0.039(44)	0[e]	∼0
g	2.000(2)	2.0[e]	2.0[e]	2.0

[a]cm^{-1}. [b]Using the 2-J Van Vleck equation. [c]2-J fit using PHI. [d]1-J fit using PHI. [e]Fixed value.

CONCLUSIONS

The use of dimethylarsinate ligands, one of the family of pseudocarboxylates, has led to the synthesis of three new polynuclear Fe^{III} oxo complexes, the first Fe clusters with arsinate ligands with nuclearity greater than two. They display a variety of binding modes, some of which also employ *anti* lone pairs and are extremely rare and/or unprecedented in Fe^{III} carboxylate chemistry. We rationalize these modes as primarily due to their high basicity and long As−O bonds compared

https://dx.doi.org/10.1021/acs.inorgchem.0c02554
Inorg. Chem. 2020, 59, 18090−18101

with carboxylate C−O bonds. As a result, μ_3- and μ_4-bridging modes are proving more common than for carboxylates.

The MSC relationship developed for high nuclearity Fe/O clusters has been found to also be applicable to Fe/oxo/arsinate clusters and helped in conjunction with DFT calculations to rationalize the observed magnetic properties of **1** and **2**; this is encouraging that the MSC can also be applied to other noncarboxylate clusters in the future. In addition, the combined use of DFT and MSC estimates of the various J_{ij} exchange interactions in **1** and **2** as inputs for fits of experimental $\chi_M T$ vs T data to give reliable J_{ij} values once again emphasizes the power of such a multipronged approach to minimize overparametrization in the study of polynuclear clusters with multiple symmetry-inequivalent J_{ij} interactions. Finally, the highly unusual structure of **3**, without a single monoatomically bridging oxo group, is another noteworthy difference between arsinate and carboxylate chemistry and promises that continued exploration of metal arsinate chemistry will lead to a variety of new structural chemistry. Further work is in progress.

■ ASSOCIATED CONTENT

Supporting Information

The Supporting Information is available free of charge at https://pubs.acs.org/doi/10.1021/acs.inorgchem.0c02554.

Tables of selected bond distances and angles and bond valence sums; infrared spectra; structural figures; ac in-phase magnetic data for **1** and **2**; and calculated spin energy plots for **1** and **2** (PDF)

Accession Codes

CCDC 2025378−2025380 contain the supplementary crystallographic data for this paper. These data can be obtained free of charge via www.ccdc.cam.ac.uk/data_request/cif, or by emailing data_request@ccdc.cam.ac.uk, or by contacting The Cambridge Crystallographic Data Centre, 12 Union Road, Cambridge CB2 1EZ, UK; fax: +44 1223 336033.

■ AUTHOR INFORMATION

Corresponding Author

George Christou − *Department of Chemistry, University of Florida, Gainesville, Florida 32611-7200, United States;* orcid.org/0000-0001-5923-5523; Email: christou@chem.ufl.edu

Authors

Kenneth Hong Kit Lee − *Department of Chemistry, University of Florida, Gainesville, Florida 32611-7200, United States*

Juan E. Peralta − *Department of Physics and Science of Advanced Materials, Central Michigan University, Mount Pleasant, Michigan 48859, United States;* orcid.org/0000-0003-2849-8472

Khalil A. Abboud − *Department of Chemistry, University of Florida, Gainesville, Florida 32611-7200, United States*

Complete contact information is available at: https://pubs.acs.org/10.1021/acs.inorgchem.0c02554

Notes

The authors declare no competing financial interest.

■ ACKNOWLEDGMENTS

This work was supported by the U.S. National Science Foundation (Grant CHE-1900321) and by the Department of Energy, Office of Science, Office of Basic Energy Sciences, as part of the Computational Chemical Sciences Program under Award #DE-SC0018331. We thank the NSF for funding of the X-ray diffractometer through grant CHE-1828064.

■ REFERENCES

(1) Gatteschi, D.; Sessoli, R.; Cornia, A. Single-Molecule Magnets Based on Iron(III) Oxo Clusters. *Chem. Commun.* **2000**, *9*, 725−732.

(2) Mitchell, K. J.; Abboud, K. A.; Christou, G. Magnetostructural Correlation for High-Nuclearity Iron(III)/Oxo Complexes and Application to Fe_5, Fe_6, and Fe_8 Clusters. *Inorg. Chem.* **2016**, *55*, 6597−6608.

(3) Cañada-Vilalta, C.; Obrien, T. A.; Brechin, E. K.; Pink, M.; Davidson, E. R.; Christou, G. Large Spin Differences in Structurally Related Fe6Molecular Clusters and Their Magnetostructural Explanation. *Inorg. Chem.* **2004**, *43*, 5505−5521.

(4) Noodleman, F.; Lovell, T.; Han, W. G.; Liu, T.; Torres, R. A.; Himo, F. Density Functional Theory. In *Comprehensive Coordination Chemistry II*; Mcleverty, J. A., Meyer, J. T., Eds.; Elsevier: 2003; Vol 2, pp 491−510, DOI: 10.1016/B0-08-043748-6/01067-7.

(5) Jian, N.; Dowle, M.; Horniblow, R. D.; Tselepis, C.; Palmer, R. E. Morphology of the Ferritin Iron Core by Aberration Corrected Scanning Transmission Electron Microscopy. *Nanotechnology* **2016**, *27*, 46LT02.

(6) Michel, F. M.; Ehm, L.; Antao, S. M.; Lee, P. L.; Chupas, P. J.; Liu, G.; Strongin, D. R.; Schoonen, M. A. A.; Phillips, B. L.; Parise, J. B. The Structure of Ferrihydrite, a Nanocrystalline Material. *Science* **2007**, *316*, 1726−1729.

(7) Sadeghi, O.; Zakharov, L. N.; Nyman, M. Aqueous Formation and Manipulation of the Iron-Oxo Keggin Ion. *Science* **2015**, *347*, 1359−1362.

(8) Chang, H.; Kim, B. H.; Jeong, H. Y.; Moon, J. H.; Park, M.; Shin, K.; Chae, S. I.; Lee, J.; Kang, T.; Choi, B. K.; Yang, J.; Bootharaju, M. S.; Song, H.; An, S. H.; Park, K. M.; Oh, J. Y.; Lee, H.; Kim, M. S.; Park, J.; Hyeon, T. Molecular-Level Understanding of Continuous Growth from Iron-Oxo Clusters to Iron Oxide Nanoparticles. *J. Am. Chem. Soc.* **2019**, *141*, 7037−7045.

(9) King, P.; Stamatatos, T. C.; Abboud, K. A.; Christou, G. Reversible Size Modification of Iron and Gallium Molecular Wheels: A Ga_{10} "Gallic Wheel" and Large Ga_{18} and Fe_{18} Wheels. *Angew. Chem., Int. Ed.* **2006**, *45*, 7379−7383.

(10) Foguet-Albiol, D.; Abboud, K. A.; Christou, G. High-Nuclearity Homometallic Iron and Nickel Clusters: Fe_{22} and Ni_{24} Complexes from the Use of N-Methyldiethanolamine. *Chem. Commun.* **2005**, *34*, 4282.

(11) Artus, P.; Boskovic, C.; Yoo, J.; Streib, W. E.; Brunel, L.-C.; Hendrickson, D. N.; Christou, G. Single-Molecule Magnets: Site-Specific Ligand Abstraction from $[Mn_{12}O_{12}(O_2CR)_{16}(H_2O)_4]$ and the Preparation and Properties of $[Mn_{12}O_{12}(NO_3)_4(O_2CCH_2{}^tBu)_{12}(H_2O)_4]$. *Inorg. Chem.* **2001**, *40*, 4199−4210.

(12) Boskovic, C.; Pink, M.; Huffman, J. C.; Hendrickson, D. N.; Christou, G. Single-Molecule Magnets: Ligand-Induced Core Distortion and Multiple Jahn−Teller Isomerism in $[Mn_{12}O_{12}(O_2CMe)_8(O_2PPh_2)_8(H_2O)_4]$. *J. Am. Chem. Soc.* **2001**, *123*, 9914−9915.

(13) Brockman, J. T.; Abboud, K. A.; Hendrickson, D. N.; Christou, G. A new family of Mn_{12} single-molecule magnets: replacement of carboxylate ligands with diphenylphosphinates. *Polyhedron* **2003**, *22*, 1765−1769.

(14) Chakov, N. E.; Wernsdorfer, W.; Abboud, K. A.; Hendrickson, D. N.; Christou, G. Single-Molecule Magnets. A Mn12 Complex with Mixed Carboxylate-Sulfonate Ligation: $[Mn_{12}O_{12}(O_2CMe)_8(O_3SPh)_8(H_2O)_4]$. *Dalton Trans.* **2003**, *11*, 2243.

(15) Chakov, N. E.; Abboud, K. A.; Zakharov, L. N.; Rheingold, A. L.; Hendrickson, D. N.; Christou, G. Reaction of $[Mn_{12}O_{12}(O_2CR)_{16}(H_2O)_4]$ single-molecule magnets with non-carboxylate ligands. *Polyhedron* **2003**, *22*, 1759−1763.
(16) Chakov, N. E.; Wernsdorfer, W.; Abboud, K. A.; Christou, G. Mixed-Valence $Mn^{III}Mn^{IV}$ Clusters $[Mn_7O_8(O_2SePh)_8(O_2CMe)(H_2O)]$ and $[Mn_7O_8(O_2SePh)_9(H_2O)]$: Single-Chain Magnets Exhibiting Quantum Tunneling of Magnetization. *Inorg. Chem.* **2004**, *43*, 5919−5930.
(17) Chakov, N. E.; Thuijs, A. E.; Wernsdorfer, W.; Rheingold, A. L.; Abboud, K. A.; Christou, G. Unusual $Mn^{III/IV}_4$ Cubane and $Mn^{III}_{16}M_4$ (M = Ca, Sr) Looplike Clusters from the Use of Dimethylarsinic Acid. *Inorg. Chem.* **2016**, *55*, 8468−8477.
(18) Konar, S.; Clearfield, A. Synthesis and Characterization of High Nuclearity Iron(III) Phosphonate Molecular Clusters. *Inorg. Chem.* **2008**, *47*, 5573−5579.
(19) Yao, H.-C.; Li, Y.-Z.; Zheng, L.-M.; Xin, X.-Q. Syntheses, Structures and Magnetic Properties of Tetra- and Heptanuclear Iron(III) Clusters Incorporating Phosphonate Ligands. *Inorg. Chim. Acta* **2005**, *358*, 2523−2529.
(20) Tolis, E. I.; Helliwell, M.; Langley, S.; Raftery, J.; Winpenny, R. E. P. Synthesis and Characterization of Iron(III) Phosphonate Cage Complexes. *Angew. Chem.* **2003**, *115*, 3934−3938.
(21) Yao, H.-C.; Wang, J.-J.; Ma, Y.-S.; Waldmann, O.; Du, W.-X.; Song, Y.; Li, Y.-Z.; Zheng, L.-M.; Decurtins, S.; Xin, X.-Q. An Iron(III) Phosphonate Cluster Containing a Nonanuclear Ring. *Chem. Commun.* **2006**, *16*, 1745.
(22) Than, R.; Schrodt, A.; Westerheide, L.; Eldik, R. V.; Krebs, B. Structural and Functional Investigations on Diiron Complexes: Catalase-Like Activity and Mechanistic Studies on the Formation of (μ-Peroxo)Diiron(III) Adducts. *Eur. J. Inorg. Chem.* **1999**, *1999*, 1537−1543.
(23) Yan, S.; Cheng, P.; Wang, Q.; Liao, D.; Jiang, Z.; Wang, G. Synthesis, Crystal Structure of Diferrous Complex and Its Reactivity with Dioxygen. *Sci. China, Ser. B: Chem.* **2000**, *43*, 405−411.
(24) Howard, P. H. *Handbook of Physical Properties of Organic Chemicals*; Meylan, W. M., Eds.; CRC Press: New York, 1997.
(25) Edmundson, R. S. *Dictionary of Organophosphorus compounds*; Chapman and Hall: London: New York, 1988.
(26) Guthrie, J. P. Hydrolysis of esters of oxy acids: pKa values for strong acids. *Can. J. Chem.* **1978**, *56*, 2342−2354.
(27) Kirkwood, R. C. *Target sites for herbicide action*; Springer Science: New York, 1991; DOI: 10.1007/978-1-4899-2433-9.
(28) Goldberg, S.; Suarez, D. Arsenate Adsorption by Unsaturated Alluvial Sediments. *Soil. Sci. Soc. Am. J.* **2013**, *77*, 782−791.
(29) Wauchope, R. D. Fixation of Arsenical Herbicides, Phosphate, and Arsenate in Alluvial Soils. *J. Environ. Qual.* **1975**, *4*, 355−358.
(30) Dickens, R.; Hiltbold, A. E. Movement and Persistence of Methanearsonates in Soil. *Weeds* **1967**, *15*, 299−304.
(31) Shimizu, M.; Arai, Y.; Sparks, D. L. Multiscale Assessment of Methylarsenic Reactivity in Soil. 1. Sorption and Desorption on Soils. *Environ. Sci. Technol.* **2011**, *45*, 4293−4299.
(32) Ona-Nguema, G.; Morin, G.; Juillot, F.; Calas, G.; Brown, G. E. EXAFS Analysis of Arsenite Adsorption onto Two-Line Ferrihydrite, Hematite, Goethite, and Lepidocrocite. *Environ. Sci. Technol.* **2005**, *39*, 9147−9155.
(33) Qi, P.; Pichler, T. Closer Look at As(III) and As(V) Adsorption onto Ferrihydrite under Competitive Conditions. *Langmuir* **2014**, *30*, 11110−11116.
(34) Huo, L.; Zeng, X.; Su, S.; Bai, L.; Wang, Y. Enhanced Removal of As(V) from Aqueous Solution Using Modified Hydrous Ferric Oxide Nanoparticles. *Sci. Rep.* **2017**, *7*, 40765.
(35) Blake, A. B.; Fraser, L. R. Crystal Structure and Mass Spectrum of μ3-Oxo-Hexakis(μ-Trimethyl-Acetato)-Trismethanoltri-Iron(III) Chloride, a Trinuclear Basic Iron(III) Carboxylate. *J. Chem. Soc., Dalton Trans.* **1975**, *3*, 193−197.
(36) Anson, C. E.; Bourke, J. P.; Cannon, R. D.; Jayasooriya, U. A.; Molinier, M.; Powell, A. K. Crystal Structures of the Isomorphous Prototypic Oxo-Centered Trinuclear Complexes. *Inorg. Chem.* **1997**, *36*, 1265−1267.
(37) *SAINT*; Bruker-AXS: Madison, WI, USA, 2013.
(38) *SHELXTL2014*; Bruker-AXS: Madison, WI, USA, 2014.
(39) Van der Sluis, P.; Spek, A. L. SQUEEZE. *Acta Crystallogr., Sect. A: Found. Crystallogr.* **1990**, *A46*, 194−201.
(40) van Wüllen, C. Broken Symmetry Approach to Density Functional Calculation of Magnetic Anisotropy or Zero Field Splittings for Multinuclear Complexes with Antiferromagnetic Coupling. *J. Phys. Chem. A* **2009**, *113*, 11535−11540.
(41) Bencini, A.; Totti, F.; Daul, C. A.; Doclo, K.; Fantucci, P.; Barone, V. Density Functional Calculations of Magnetic Exchange Interactions in Polynuclear Transition Metal Complexes. *Inorg. Chem.* **1997**, *36*, 5022−5030.
(42) Ruiz, E.; Rodriguez-Fortea, A.; Cano, A.; Alvarez, S.; Alemany, P. About the calculation of exchange coupling constants in polynuclear transition metal complexes. *J. Comput. Chem.* **2003**, *24*, 982−989.
(43) Valero, R.; Costa, R.; Moreirra, I. R.; Truhlar, D. G.; Illas, F. Performance of the M06 family of exchange-correlation functionals for predicting magnetic coupling in organic and inorganic molecules. *J. Chem. Phys.* **2008**, *128*, 114103.
(44) Comba, P.; Hausberg, S.; Martin, B. Calculation of Exchange Coupling Constants of Transition Metal Complexes with DFT. *J. Phys. Chem. A* **2009**, *113*, 6751−6755.
(45) Phillips, J. J.; Peralta, J. E. Magnetic Exchange Couplings from Semilocal Functionals Evaluated Nonself-Consistently on Hybrid Densities: Insights on Relative Importance of Exchange, Correlation, and Delocalization. *J. Chem. Theory Comput.* **2012**, *8*, 3147−3158.
(46) Joshi, R. P.; Phillips, J. J.; Mitchell, K. J.; Christou, G.; Jackson, K. A.; Peralta, J. E. Accuracy of density functional theory methods for the calculation of magnetic exchange couplings in binuclear iron(III) complexes. *Polyhedron* **2020**, *176*, 114194.
(47) Krishnan, R.; Binkley, J. S.; Seeger, R.; Pople, J. A. Self-consistent molecular orbital methods. XX. A basis set for correlated wave functions. *J. Chem. Phys.* **1980**, *72*, 650.
(48) Blaudeau, J. Extension of Gaussian-2 (G2) theory to molecules containing third-row atoms K and Ca. *J. Chem. Phys.* **1997**, *107*, 5016.
(49) Frisch, M. J.; Trucks, G. W.; Schlegel, H. B.; Scuseria, G. E.; Robb, M. A.; Cheeseman, J. R.; Scalmani, G.; Barone, V.; Petersson, G. A.; Nakatsuji, H.; Li, X.; Caricato, M.; Marenich, A. V.; Bloino, J.; Janesko, B. G.; Gomperts, R.; Mennucci, B.; Hratchian, H. P.; Ortiz, J. V.; Izmaylov, A. F.; Sonnenberg, J. L.; Williams-Young, D.; Ding, F.; Lipparini, F.; Egidi, F.; Goings, J.; Peng, B.; Petrone, A.; Henderson, T.; Ranasinghe, D.; Zakrzewski, V. G.; Gao, J.; Rega, N.; Zheng, G.; Liang, W.; Hada, M.; Ehara, M.; Toyota, K.; Fukuda, R.; Hasegawa, J.; Ishida, M.; Nakajima, T.; Honda, Y.; Kitao, O.; Nakai, H.; Vreven, T.; Throssell, K.; Montgomery, J. A., Jr.; Peralta, J. E.; Ogliaro, F.; Bearpark, M. J.; Heyd, J. J.; Brothers, E. N.; Kudin, K. N.; Staroverov, V. N.; Keith, T. A.; Kobayashi, R.; Normand, J.; Raghavachari, K.; Rendell, A. P.; Burant, J. C.; Iyengar, S. S.; Tomasi, J.; Cossi, M.; Millam, J. M.; Klene, M.; Adamo, C.; Cammi, R.; Ochterski, J. W.; Martin, R. L.; Morokuma, K.; Farkas, O.; Foresman, J. B.; Fox, D. J. *Gaussian 16*, Revision C.01; Gaussian, Inc.: Wallingford, CT, 2016.
(50) Chilton, N. F.; Anderson, R. P.; Turner, L. D.; Soncini, A.; Murray, K. S. PHI: A Powerful New Program for the Analysis of Anisotropic Monomeric and Exchange-Coupled Polynuclear d- and f-Block Complexes. *J. Comput. Chem.* **2013**, *34*, 1164−1175.
(51) Brown, I. D.; Altermatt, D. Bond-valence parameters obtained from a systematic analysis of the Inorganic Crystal Structure Database. *Acta Crystallogr., Sect. B: Struct. Sci.* **1985**, *B41*, 244−247.
(52) Kufareva, I.; Abagyan, R. Methods of protein structure comparison. *Homology Modeling. Methods in Molecular Biology (Methods and Protocols)*; 2011; Vol. *857*, pp 231−257,.
(53) (a) Christmas, C. A.; Tsai, H. L.; Pardi, L.; Kesselman, J. M.; Gantzel, P. K.; Chadha, R. K.; Gatteschi, D.; Harvey, D. F.; Hendrickson, D. N. Hexanuclear Ferric Complexes Possessing Different Degrees of Spin Frustration. *J. Am. Chem. Soc.* **1993**, *115*, 12483−12490. (b) Jones, L. F.; Jensen, P.; Moubaraki, B.; Cashion, J.

D.; Berry, K. J.; Murray, K. S. The role of diisopropanolamine ($dipaH_3$) in cluster dimerisation and polymerisation: from spin frustrated $S = 5$ Fe^{III}_6 clusters to the novel 1-D covalent polymer of mixed valence $[Co^{II}_3Co^{III}]$ tetramers. *Dalton Trans.* **2005**, 3344−3352. (c) Cañada-Vilalta, C.; Rumberger, E.; Brechin, E. K.; Wernsdorfer, W.; Folting, K.; Davidson, E. R.; Hendrickson, D. N.; Christou, G. Two new hexanuclear iron(III) complexes with $S = 5$ ground states. *J. Chem. Soc., Dalton Trans.* **2002**, 4005−4010. (d) Yoon, S.; Lippard, S. J. Water Affects the Stereochemistry and Dioxygen Reactivity of Carboxylate-Rich Diiron(II) Models for the Diiron Centers in Dioxygen-Dependent Non-Heme Enzymes. *J. Am. Chem. Soc.* **2005**, *127*, 8386−8397.

(54) (a) Çelenligil-Çetin, R.; Staples, R. J.; Stavropoulos, P. Synthesis, Characterization, and Reactivity of Ferrous and Ferric Oxo/Peroxo Pivalate Complexes in Relation to Gif-Type Oxygenation of Substrates. *Inorg. Chem.* **2000**, *39*, 5838−5846. (b) Saalfrank, R. W.; Bernt, I.; Chowdhry, M. M.; Hampel, F.; Vaughan, G. B. M. Ligand-to-Metal Ratio Controlled Assembly of Tetra- and Hexanuclear Clusters Towards Single-Molecule Magnets. *Chem. - Eur. J.* **2001**, *7*, 2765−2769. (c) Murugesu, M.; Abboud, K. A.; Christou, G. Preparation and properties of new Fe_6 and Fe_8 clusters of iron(III) with tripodal ligands. *Dalton Trans.* **2003**, 4552−4556. (d) Saalfrank, R. W.; Deutscher, C.; Sperner, S.; Nakajima, T.; Ako, A. M.; Uller, E.; Hampel, F.; Heinemann, F. W. Six-Membered Metalla-coronands. Synthesis and Crystal Packing: Columns, Compartments, and 3D-Networks. *Inorg. Chem.* **2004**, *43*, 4372−4382. (e) Koizumi, S.; Nihei, M.; Nakano, M.; Oshio, H. Antiferromagnetic Fe^{III}_6 Ring and Single-Molecule Magnet $Mn^{II}_3Mn^{III}_4$ Wheel. *Inorg. Chem.* **2005**, *44*, 1208−1210. (f) Smith, A. A.; Coxall, R. A.; Harrison, A.; Helliwell, M.; Parsons, S.; Winpenny, R. E. P. High-temperature synthesis of polynuclear iron oxo-hydroxy complexes. *Polyhedron* **2004**, *23*, 1557−1565. (g) Ammala, P. S.; Cashion, J. D.; Kepert, C. M.; Murray, K. S.; Moubaraki, B.; Spiccia, L.; West, B. O. The synthesis, structure, magnetic and Mössbauer spectral properties of an Fe−Zr carboxylate−alkoxide derivative containing an $\{Fe_2Zr_2(\mu_3\text{-}O)_2\}$ core. *J. Chem. Soc., Dalton Trans.* **2001**, 2032−2041.

(55) (a) Shweky, I.; Pence, L. E.; Papaefthymiou, G. C.; Sessoli, R.; Yun, J. W.; Bino, A.; Lippard, S. J. A Hexairon(III) Complex with Three Nonplanar η^2-μ_4-Peroxo Ligands Bridging Two Basic Iron Acetate Units. *J. Am. Chem. Soc.* **1997**, *119*, 1037−1042. (b) Schneppensieper, T.; Liehr, G.; van Eldik, R.; Ensling, J.; Gütlich, P. A New Cylindrical, Six-Membered Iron(III) Inclusion Cluster Consisting of Three Oxo-Bridged Diiron Subunits Linked by Carboxylate Bridges. *Inorg. Chem.* **2000**, *39*, 5565−5568. (c) Saalfrank, R. W.; Glaser, H.; Demleitner, B.; Hampel, F.; Chowdhry, M. M.; Schünemann, V.; Trautwein, A. X.; Vaughan, G. B. M.; Yeh, R.; Davis, A. V.; Raymond, K. N. Self-Assembly of Tetrahedral and Trigonal Antiprismatic Clusters $[Fe_4(L^4)_4]$ and $[Fe_6(L^5)_6]$ on the Basis of Trigonal Tris-Bidentate Chelators. *Chem. - Eur. J.* **2002**, *8*, 493−497. (d) Harding, C. J.; Henderson, R. K.; Powell, A. K. A New Type of Hexanuclear Iron(III) Hydroxo(oxo) Cluster. *Angew. Chem., Int. Ed. Engl.* **1993**, *32*, 570−572.

(56) (a) Raptopoulou, C. P.; Boudalis, A. K.; Sanakis, Y.; Psycharis, V.; Clemente-Juan, J. M.; Fardis, M.; Diamantopoulos, G.; Papavassiliou, G. Hexanuclear Iron(III) Salicylaldoximato Complexes Presenting the $[Fe_6(\mu_3\text{-}O)_2(\mu_2\text{-}OR)_2]_{12}$ Core: Syntheses, Crystal Structures, and Spectroscopic and Magnetic Characterization. *Inorg. Chem.* **2006**, *45*, 2317−2326. (b) Saalfrank, R. W.; Reimann, U.; Göritz, M.; Hampel, F.; Scheurer, A.; Heinemann, F. W.; Büschel, M.; Daub, J.; Schünemann, V.; Trautwein, A. X. Metal- and Ligand-Directed One-Pot Syntheses, Crystal Structures, and Properties of Novel Oxo-Centered Tetra- and Hexametallic Clusters. *Chem. - Eur. J.* **2002**, *8*, 3614−3619. (c) Tolis, E. I.; Helliwell, M.; Langley, S.; Raftery, J.; Winpenny, R. E. P. Synthesis and Characterization of Iron(III) Phosphonate Cage Complexes. *Angew. Chem., Int. Ed.* **2003**, *42*, 3804. (d) Gerbeleu, N. V.; Batsanov, A. S.; Timko, G. A.; Struchkov, Y. T.; Indrichan, K. M.; Popovich, G. A. Synthesis and structure of trinuclear and hexanuclear μ_3-oxopivalates of Iron(III). *Dokl. Akad. Nauk SSSR (Russ.).* **1987**, *293*, 364.

(57) (a) Cornia, A.; Gatteschi, D.; Hegetschweiler, K.; Hausherr-Primo, L.; Gramlich, V. Metal Binding of Polyalcohols. 4. Structure and Magnetism of the Hexanuclear, μ_6-Oxo-Centered $[OFe_6(H_3thme)_3(OCH_3)_3Cl_6]^{2-}$ (H_3thme = 1,1,1-Tris-(Hydroxymethyl)Ethane). *Inorg. Chem.* **1996**, *35*, 4414−4419. (b) Hegetschweiler, K.; Schmalle, H. W.; Streit, H. M.; Gramlich, V.; Hund, H.-U.; Erni, I. A simple, efficient route to a μ_6-oxo-centered hexanuclear iron(III) alkoxide complex: preparation and structure of $Na_2Fe_6O(OCH_3)_{18}.6CH_3OH$. *Inorg. Chem.* **1992**, *31*, 1299−1302. (c) Hegetschweiler, K.; Schmalle, H. W.; Streit, H. M.; Schneider, W. Synthesis and structure of a novel hexanuclear iron(III) complex containing six terminal and twelve bridging groups and one μ_6-oxo bridge. *Inorg. Chem.* **1990**, *29*, 3625−3627.

(58) (a) Burkill, H. A.; Robertson, N.; Vilar, R.; White, A. J. P.; Williams, D. J. Synthesis, Structural Characterization, and Magnetic Studies of Polynuclear Iron Complexes with a New Disubstituted Pyridine Ligand. *Inorg. Chem.* **2005**, *44*, 3337−3346. (b) Seddon, E. J.; Huffman, J. C.; Christou, G. A new core topology in hexanuclear iron(III) carboxylate chemistry: $[Fe_6O_3(O_2CMe)_9(OEt)_2(bpy)_2](ClO_4)$. *J. Chem. Soc., Dalton Trans.* **2000**, 4446−4452. (c) Seddon, E. J.; Yoo, J.; Folting, K.; Huffman, J. C.; Hendrickson, D. N.; Christou, G. Dinuclear and hexanuclear iron(m) carboxylate clusters with a bis(bipyridine) ligand: Supramolecular aggregation of $[Fe_2O_2]$ units to give a $[Fe_6O1]$ ladder structure. *J. Chem. Soc., Dalton Trans.* **2000**, 3640−3648. (d) Nair, V. S.; Hagen, K. S. Iron oxo aggregation: Fe3 to Fe6. Synthesis, structure, and magnetic properties of the hexanuclear dication $[Fe_6(\mu_4\text{-}O)_2(\mu_2\text{-}OMe)_8(OMe)_4(tren)_2]^{2+}$, a soluble, crystalline model of iron oxo hydroxo nanoparticles, the core of ferritin and rust formation. *Inorg. Chem.* **1992**, *31*, 4048−4050.

(59) Thuijs, A.; Li, X.; Wang, Y.; Abboud, K.; Zhang, X.; Cheng, H.; Christou, G. Molecular Analogue of the Perovskite Repeating Unit and Evidence for Direct Mn^{III}-Ce^{IV}-Mn^{III} Exchange Coupling Pathway. *Nat. Commun.* **2017**, *8*, 500.

(60) Schmitt, W.; Anson, C.; Hill, J.; Powell, A. Cation−π Binding of an Alkali Metal Ion by Pendant A, A-Dimethylbenzyl Groups Within A Dinuclear Iron(III) Structural Unit. *J. Am. Chem. Soc.* **2003**, *125*, 11142−11143.

(61) Angaridis, P.; Kampf, J.; Pecoraro, V. Multinuclear Fe(III) Complexes with Polydentate Ligands of the Family of Dicarboxyimidazoles: Nuclearity- and Topology-Controlled Syntheses and Magneto-Structural Correlations. *Inorg. Chem.* **2005**, *44*, 3626−3635.

(62) Lachicotte, R. J.; Hagen, K. S. Synthesis and Structures of Trinuclear and μ-Hydroxo Pentanuclear Iron(II) Carboxylates as Models of Reduced Ferritin and White Rust. *Inorg. Chim. Acta* **1997**, *263*, 407−414.

(63) Reisner, E.; Telser, J.; Lippard, S. J. A Planar Carboxylate-Rich Tetrairon(II) Complex and its Conversion to Linear Triiron(II) and Paddlewheel Diiron(II) Complexes. *Inorg. Chem.* **2007**, *46*, 10754−10770.

(64) Peterson, M. R.; Csizmadia, I. G. Determination and Analysis of the Formic Acid Conformational Hypersurface. *J. Am. Chem. Soc.* **1979**, *101*, 1076−1079.

(65) Gandour, R. D. On the Importance of Orientation in General Base Catalysis by Carboxylate. *Bioorg. Chem.* **1981**, *10*, 169−176.

(66) Silberberg, M. S. *Chemistry: the molecular nature of matter and change*, 6th ed.; McGraw-Hill Science: Boston, 2012.

(67) Carrell, C. J.; Carrell, H. L.; Erlebacher, J.; Glusker, J. P. Structural Aspects of Metal Ion Carboxylate Interactions. *J. Am. Chem. Soc.* **1988**, *110*, 8651−8656.

(68) Konar, S.; Bhuvanesh, N.; Clearfield, A. Oxo-, Hydroxo-, and Peroxo-Bridged Fe(III) Phosphonate Cages. *J. Am. Chem. Soc.* **2006**, *128*, 9604−9605.

(69) Belli Dell'Amico, D.; Boschi, D.; Calderazzo, F.; Ianelli, S.; Labella, L.; Marchetti, F.; Pelizzi, G.; Quadrelli, E. N,N-Dialkylcarbamato M-Oxo Derivatives Of Iron(III). *Inorg. Chim. Acta* **2000**, *300*−*302*, 882−891.

(70) Weihe, H.; Güdel, H. U. Angular and Distance Dependence of the Magnetic Properties of Oxo-Bridged Iron(III) Dimers. *J. Am. Chem. Soc.* **1997**, *119*, 6539−6543.

https://dx.doi.org/10.1021/acs.inorgchem.0c02554
Inorg. Chem. 2020, 59, 18090−18101

(71) Wang, G. X.; Hua, Z.; Yao, C.; Tian, Y. Y.; De, G. F. Studies on ohe Magnetic Property of M_3-Oxotriiron(III) Complex $[Fe_3O(OBz)_6(CH_3OH)_3](NO_3)(CH_3OH)_2$ (HOBz = benzoic Acid). *Chin. J. Chem.* **1996**, *14*, 200−205.
(72) Boudalis, A.; Sanakis, Y.; Dahan, F.; Hendrich, M.; Tuchagues, J. An Octanuclear Complex Containing The $\{Fe_3O\}^{7+}$ Metal Core: Structural, Magnetic, Mössbauer, And Electron Paramagnetic Resonance Studies. *Inorg. Chem.* **2006**, *45*, 443−453.
(73) Kambe, K. On the Paramagnetic Susceptibilities of Some Polynuclear Complex Salts. *J. Phys. Soc. Jpn.* **1950**, *5*, 48−51.

https://dx.doi.org/10.1021/acs.inorgchem.0c02554
Inorg. Chem. 2020, 59, 18090−18101